adsorbed by the exterior surfaces of SWNTs and/or the interstitial spaces between bundled tubes.

A vehicle powered by a fuel cell would require ~3.1 kg of H_2 for a 500 km range[17]. This amount of H_2 stored in the weight and volume of a typical petrol tank requires system densities approaching 6.5 wt% and 62 kg H_2 m^{-3} (ref. 17). Figure 2 shows that no storage technology is currently capable of meeting these goals. SWNTs with diameters of 16.3 Å and 20 Å would come close to the target densities and operate near room temperatures if modest H_2 over-pressures compensated for the lower heats of adsorption expected in the larger cavities. These materials would have high energy storage efficiencies as they would operate at or near ambient temperatures and pressures. In contrast, 25 to 45% of the energy content in liquefied H_2 is required for liquefaction[18], and ~9% of the stored energy is needed for compression of H_2 to 20 MPa (ref. 17). For catalytic generation of H_2 by the reaction of H_2O with iron, temperatures in excess of 250 °C are required[17,19].

The effect of hydrogen over-pressure on the stability of adsorbed H_2 has not yet been investigated and remains an important question. The high-purity 13.8-Å diameter SWNT samples that have recently been produced by laser vaporization[20] should be interesting candidates for evaluation. The temperature and pressure requirements for H_2 adsorption and desorption, and the kinetics for charging and discharging, are expected to be a function of nanotube diameter and aspect ratio. Control of these parameters coupled with improvements in production, purification and alignment of SWNTs may lead to a new H_2 storage technology for hydrogen-fuelled vehicles with superior performance to currently available options. □

Received 4 November 1996; accepted 10 February 1997.

1. Gregg, S. J. & Sing, K. S. W. *Adsorption, Surface Area and Porosity* (Academic, London, 1982).
2. Pederson, M. R. & Broughton, J. Q. Nanocapillarity in fullerene tubules. *Phys. Rev. Lett.* **69,** 2689–2692 (1992).
3. Dujardin, E., Ebbesen, T. W., Hiura, H. & Tanigaki, K. Capillarity and wetting of carbon nanotubes. *Science* **265,** 1850–1852 (1994).
4. Bethune, D. S. *et al.* Cobalt-catalysed growth of carbon nanotubes with single-atomic-layer walls. *Nature* **363,** 605–607 (1993).
5. Pace, E. L. & Siebert, A. R. Heat of adsorption of parahydrogen and orthodeuterium on graphon. *J. Phys. Chem.* **63,** 1398–1400 (1959).
6. Bandosz, T. J., Jagiello, J., Amankwah, K. A. G. & Schwarz, J. A. Chemical and structural properties of clay minerals modified by inorganic and organic material. *Clay Miner.* **27,** 435–444 (1992).
7. Schwarz, J. A. *Final Report for the Tasks XC-1-1108-1 and XAE-3-13346-01* (National Renewable Energy Laboratory, Golden, Colorado, 1994).
8. Dillon, A. C., Bekkedahl, T. A., Cahill, A. E., Jones, K. M. & Heben, M. J. Carbon nanotube materials for hydrogen storage. *Proc. 1995 U.S. DOE Hydrogen Program Review* 521–541 (National Renewable Energy Laboratory, Golden, Colorado, 1995).
9. Madix, R. J. The application of flash desorption spectroscopy to chemical reactions on surfaces: Temperature programmed reaction spectroscopy. *Chemistry and Physics of Solid Surfaces* (ed. Vanselov, R.) 63–72 (CRC, Boca Raton, 1979).
10. Ibok, E. E. & Ollis, D. F. Temperature programmed desorption from porous catalysts: Shape index analysis. *J. Catal.* **66,** 391–400 (1980).
11. Peterson, B. K. & Gubbins, K. E. Phase transitions in a cylindrical pore: Grand canonical Monte Carlo, mean field theory, and the Kelvin equation. *Molec. Phys.* **62,** 215–226 (1987).
12. Ajayan, P. M. *et al.* Opening carbon nanotubes with oxygen and implications for filling. *Nature* **362,** 522–525 (1993).
13. Tsang, S. C., Harris, P. J. F. & Green, M. L. H. Thinning and opening of carbon nanotubes by oxidation using carbon dioxide. *Nature* **362,** 520–522 (1993).
14. Ernst, K. H., Schwarz, E. & Christmann, K. The interaction of hydrogen with a cobalt (1010) surface. *J. Chem. Phys.* **101,** 5388–5401 (1994).
15. Lisowski, W. The kinetics of the low-temperature hydrogen interaction with polycrystalline cobalt films. *Appl. Surf. Sci.* **37,** 272–282 (1989).
16. Nielsen, M., McTague, J. P. & Ellenson, W. Adsorbed layers of D_2, H_2, O_2, and ^3He on graphite studied by neutron scattering. *J. Phys.* **38,** C4/10–C4/18 (1977).
17. DeLuchi, M. *Hydrogen Fuel-Cell Vehicles* (Institute of Transportation Studies, Univ. California, Davis, 1992).
18. DeLuchi, M. A. Hydrogen vehicles: An evaluation of fuel storage, performance, safety, environmental impacts, and cost. *Int. J. Hydrogen Energy* **14,** 81–130 (1989).
19. T-Raissi, A. & Sadhu, A. Systems study of metal hydride storage requirements. *Proc. 1994 DOE/NREL Hydrogen Program Review* 85–106 (National Renewable Energy Laboratory, Golden, Colorado, 1994).
20. Thess, A. *et al.* Crystalline ropes of metallic carbon nanotubes. *Science* **273,** 483–487 (1996).
21. Gordon, R. Composite pressure vessels for gaseous hydrogen-powered vehicles. *Hydrogen Energy Progress V* (eds Veziroglu, T. N. Taylor, J. B.) 1225–1236 (Pergamon, New York, 1984).
22. Dresselhaus, M. S., Dresselhaus, G. & Saito, R. C_{60} related tubules. *Solid State Commun.* **84,** 201–205 (1992).

Acknowledgements. We thank Jeremy Broughton, J. Karl Johnson and Al Czanderna for technical discussions. We also thank Spectracorp Limited for activated carbon samples, and A. Mason for microprobe measurements. This work was funded by the US Department of Energy Hydrogen Program.

Correspondence and requests for materials should be addressed to M.J.H. (e-mail: mikeh@nrel.gov).

Spontaneous stratification in granular mixtures

Hernán A. Makse*, Shlomo Havlin*†, Peter R. King‡ & H. Eugene Stanley*

* *Center for Polymer Studies and Physics Department, Boston University, Boston, Massachusetts 02215, USA*

† *Minerva Center and Department of Physics, Bar-Ilan University, Ramat Gan, Israel*

‡ *BP Exploration Operating Company Ltd, Sunbury-on-Thames, Middlesex, TW16 7LN, UK*

Granular materials[1–5] segregate according to grain size when exposed to periodic perturbations such as vibrations[6–12]. Moreover, mixtures of grains of different sizes can also spontaneously segregate in the absence of external perturbations: when such a mixture is simply poured onto a pile, the large grains are more likely to be found near the base, while the small grains are more likely to be near the top[13–20]. Here we report another size-separation effect, which arises when we pour a granular mixture between two vertical plates: the mixture spontaneously stratifies into alternating layers of small and large grains whenever the large grains have larger angle of repose than the small grains. We find only spontaneous segregation, without stratification, when the large grains have smaller angle of repose than the small grains. The stratification is related to the occurrence of avalanches: during each avalanche, the grains separate into a pair of static layers, with the small grains forming a sublayer underneath the layer of large grains.

Our experimental system consists of a vertical 'quasi-two-dimensional' cell with a gap of 5 mm separating two transparent plates (made of Plexiglass or glass) measuring 300 mm × 200 mm (Fig. 1a). To avoid the effects of electrostatic interactions between the grains and the wall, the wall is cleaned with an antistatic cleaner.

In a first series of experiments, we closed the left edge of the cell leaving the right edge free, and we poured, near the left edge, an equal-volume mixture of white glass beads (mean size 0.27 mm, spherical shape, repose angle 26°), and red sugar crystals (typical size 0.8 mm, cubic shape, repose angle 39°). Figure 1a shows the result of the first series of experiments. We note two features: (1) Spontaneous stratification. We see the formation of alternating layers consisting of small and large grains—with a 'wavelength' of ~1.2 cm. (2) Spontaneous segregation. We find that the smaller grains segregate near the left edge and the larger grains segregate furthest from it and near the base[13–20].

In a second series of experiments, we confirmed the results of these initial experiments by testing for stratification and segregation using a mixture of grains of same density, consisting of fine sand (typical size 0.4 mm) and coarse sand (typical size 1 mm), suggesting that the density of the grains may not play an important role in stratification.

In all the above experiments we used mixtures composed of two types of grain with different shape, and therefore with different angles of repose. In particular we obtained stratification (plus segregation) when we used larger cubic grains and smaller spherical grains: the angle of repose of the large species was then larger than the angle of repose of the small species. Otherwise we obtained only segregation and not stratification when the large grains were less faceted than the small grains, that is, the large grains had smaller angle of repose than the small grains.

To confirm this, we performed a series of experiments using mixtures of irregular shaped sand grains (repose angle 35°, mean size 0.3 mm), and spherical glass beads (repose angle 26° smaller than the repose angle of the sand grains). We found that stratification

(plus segregation) occurred for two different experiments using spherical beads of size 0.07 mm and 0.11 mm (so that the larger grains had larger repose angle). In contrast, we obtained only segregation but not stratification for two experiments using spherical beads of size 0.55 mm and 0.77 mm (so that the larger grains had smaller repose angle). In all cases the segregation of grains occurred with the smaller grains being found near the left edge of the cell and the larger grains near the base of the cell. These results suggest that the phenomenon of segregation is always expected when pouring a granular mixture of grains of different sizes, no matter what are the values of the angles of repose of the species. However, the phenomenon of stratification is only expected when the large species have larger angle of repose than the small species.

Additionally, we performed a series of experiments (not shown) in which we found similar stratification by using different mixtures of differing size ratio between large and small grains (1.66, 2.1, 2.25, 3.25 and 6.66), suggesting that the phenomenon occurs for a broad regime of grain size ratios. We found a similar stratification when we doubled the gap between the vertical plates of the cell and simultaneously doubled the flow rate of grains.

We propose a physical mechanism responsible for the observed stratification that is related to the fact that not one but rather a pair of layers is formed in the course of each avalanche. When the flow of grains reaches the base of the pile, we find that the grains develop a profile characterized by a well-defined 'kink', at which the grains are stopped (Fig. 1b); but we find that the small grains stop first, so a pair of layers forms with the small grains underneath the large grains. As more grains are added, the kink appears to move upwards in the direction opposite to the flow of grains. Once the kink reaches the top, the pair of layers is complete and the cycle is then repeated: a new avalanche occurs, the kink develops, and a new pair of layers forms.

The 'wavelength' of a pair of layers λ can be determined by the mean value of the downward velocity v of the rolling grains during an avalanche, the upward velocity v' of the kink, and the thickness of the layer of rolling grains R_0 during the avalanche. If the volume of grains in an avalanche scales approximately as the volume of grains in a well formed kink, we predict $\lambda \approx R_0(v + v')/v'$, and we confirm this relation experimentally.

To test this physical mechanism by computer simulation we

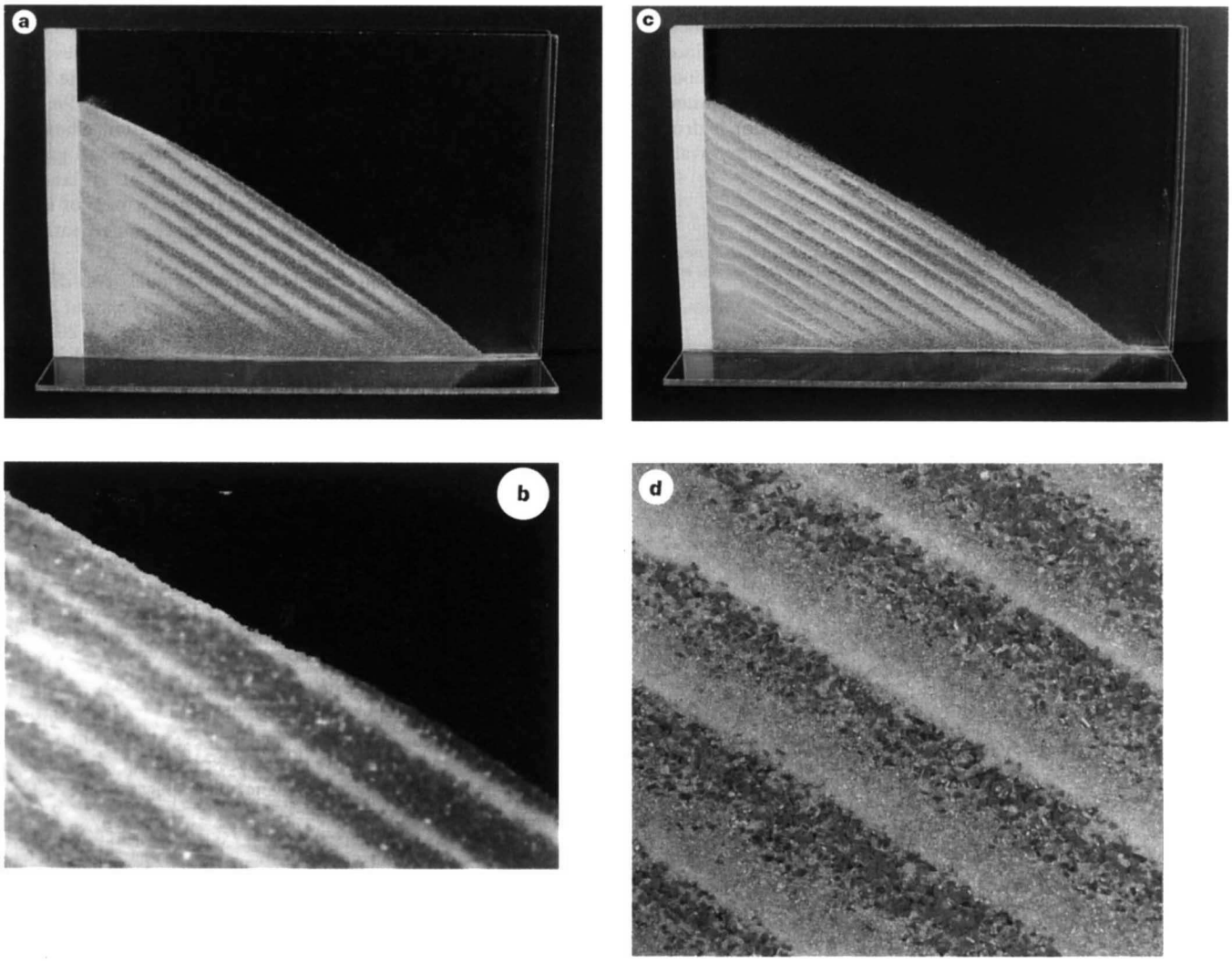

Figure 1 Experimental results. **a**, Typical result of the first series of experiments, showing the formation of successive layers of fine and coarse grains (here the white grains are glass beads of average diameter 0.27 mm, while the larger grains are sugar crystals of typical size 0.8 mm). We poured the equal-volume mixture near the left edge between two transparent vertical plates separated by a gap of 5 mm. We obtained statification with a wavelength $\lambda \approx 1.2$ cm. **b**, Close-up photograph of the kink where the grains stop during an avalanche. The small white grains stop first, and then the large red grains; hence the small grains form a sublayer underneath the large grains. **c**, Stratification obtained using a mixture of three different types of grains: nearly spherical glass beads (0.15 mm, angle of repose 26°), blue sand (0.4 mm, angle of repose 35°) and red sugar crystals (0.8 mm, angle of repose 39°). We notice the grading (from bottom to top) in a triplet of layers: small (white), medium (blue) and large (red) grains. **d**, Close-up photograph of the stratification pattern of **c**, field of view 40 mm × 40 mm.

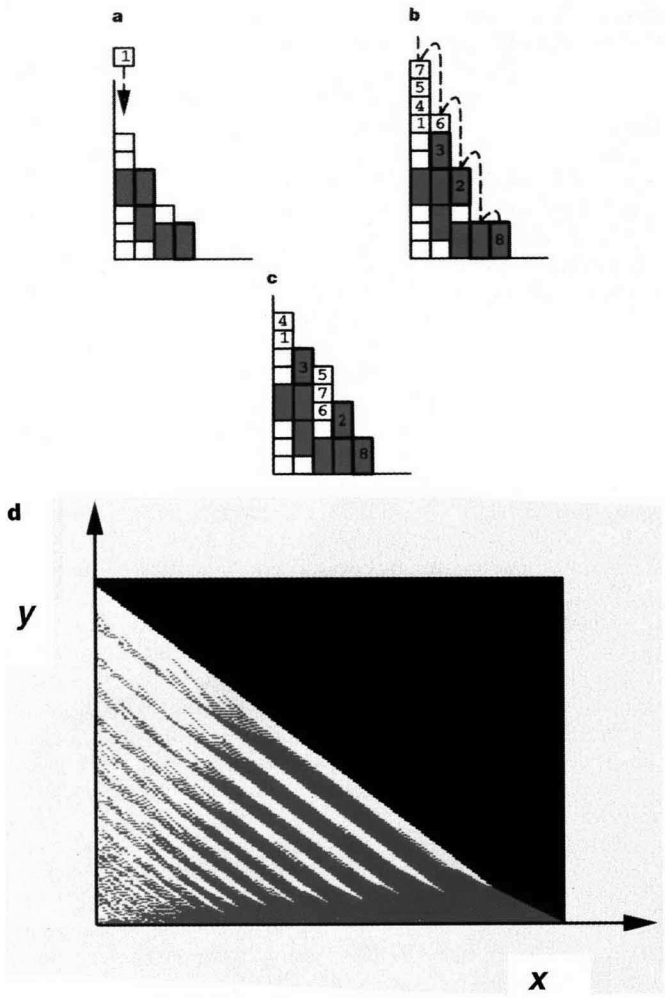

Figure 2 Results of modelling. **a**, The dynamics of the simplest 'mean field' model are illustrated by this example with two sizes $H_1 = 1$ (white) and $H_2 = 2$ (red), and threshold slopes $s_r \equiv \tan\theta_r = 2$ and $s_m \equiv \tan\theta_m = 3$. Suppose that, at a given instant, the sand pile is at the critical slope for repose s_r. To define the dynamical rules for the arriving grains, we consider the slope $s_i \equiv h_i - h_{i+1}$, where h_i denotes the height of the sand pile at coordinate i. We deposit a grain near the first column at the left edge of the lattice, where the actual column position is chosen from a narrow gaussian probability distribution centred at the wall edge. The non-zero width of this gaussian mirrors the fact that grains often bounce after reaching the pile. Newly arriving grains accumulate on the sand pile profile, following dynamics governed by the critical slope s_m; thus a grain moves from the initial landing point at column i to column $i + 1$ if the slope $h_i - h_{i+1}$ is larger than s_m, then moves from column $i + 1$ to column $i + 2$ if $h_{i+1} - h_{i+2} > s_m$, and so forth. The grain stops at the first column k with $h_k - h_{k+1} \leq s_m$. Another grain is now added, and the same rules are followed. **b**, This entire process continues until a grain reaches the substrate at the furthest right column of the pile for first time (grain 8 in this figure). Now, as $s_i > s_m$ for all columns i, the sand pile has become 'unstable'. We note that s_i is calculated considering also the size of the rolling grain; as a result, the large grains more readily reach a slope that exceeds the two critical slopes s_r and s_m. **c**, We allow the sand pile to relax towards the repose slope s_r by moving each of the grains with slope larger than s_r to the nearest column satisfying $h_i - h_{i+1} \leq s_r$. Now the deposition starts again, and we iterate the algorithm until a large sand pile (of typically 10^5 grains) is formed. We can obtain stratification with constant 'wavelength' by stopping the accumulation process when a grain reaches for first time the column $l^{1/2}$, where l denotes the furthest-right column of the pile. **d**, Image obtained with the simplest 'mean field' model (for parameters $H_1 = 1$, $H_2 = 2$, $s_r = 4$ and $s_m = 5$); the smaller grains are white and the larger grains red. We find stratification and also reproduce the 'kink' mechanism explained in the text when we improve upon the simplest 'mean field' model by including four different angles of repose to take into account the fact that the angle of repose depends on the concentration of grains at the surface of the pile[23].

considered a mixture comprising small grains of width one pixel and of height H_1, and large grains, also of width one pixel but of height $H_2 > H_1$. To generate an equal-volume mixture, we randomly 'dropped' a small grain with probability $p \equiv H_2/(H_1 + H_2)$, and 'dropped' a large grain with probability $1 - p$ (Fig. 2).

In critical phenomena, it is often useful to first develop a 'mean field' type model (in which, for example, spin orientation is determined by a macroscopic variable, the net magnetization), before devising models in which spin orientation is determined by the microscopic quantities such as the orientations of the other spins comprising the system. In this spirit, we focus first not on the 'microscopic' grain motions, but rather on the 'macroscopic' angle of the sand pile, whose value alternates in time between the maximum angle of stability θ_m which defines the onset of an avalanche, and the angle of repose θ_r which defines the end of the avalanche[21,22]. Using this model (described in Fig. 2 legend), we found a morphology that displays both segregation and stratification.

In addition to the simplest 'mean field' approach, we developed a model[23] in which we treat the individual grain motion in accordance with microscopic rules that depend not on the macroscopic angle of the sand pile, but rather on the local angles formed between each grain and its neighbours. Specifically, the dynamics of the small and large rolling grains are governed by the critical angles of repose corresponding to the interactions between the rolling grain and the static grains of the sand-pile surface. This model incorporates the experimental fact that grains segregate because large grains roll down more easily on top of small grains than small grains on top of large grains (for rolling large grains on top of a surface of small grains, the surface appears smoother than for rolling small grains on top of a surface of large grains). Thus the model correctly predicts that the small grains form a sublayer beneath the large grains. We find stratification, as in the simplest 'mean field' model, and also find that the profile of the sandpile displays a kink at which rolling grains are stopped—just as in the experiment.

Next we tested the above principles by generalizing from two grain sizes to three. The experiment resulted in stratification with three layers, with the finest grains on the bottommost of each triplet of layers and the coarsest grains on the topmost layer (see Fig. 1c where the same experimental setup of Fig. 1a is used to obtain an alternation of three layers of grains of three different sizes: 0.15 mm, 0.4 mm and 0.8 mm; a close-up view of the stratification pattern of Fig. 1c is shown in Fig. 1d). We are now performing experiments using a continuum size distribution, as geological rock formations (which also display stratification) generally occur in the presence of a continuum distribution of grain size.

To provide another test of the proposed physical mechanism, we note that if both grains are spherical, there should be no stratification because the angles of repose of the large and small grains are then the same. We confirmed this expectation experimentally. The case of spherical grains was also studied by Williams[24–26], who seems to have seen a hint of the stratification effect. However, its origin in that case appears to have been an artefact, presumably because his grains were in fact of slightly different shapes.

We note that Boutreux and de Gennes have recently made considerable progress[27] in developing a general theoretical framework[28,29] to treat the case of granular flows of two different grains. Their conclusions[27–29] are consistent with the experiments presented here. □

Received 11 October 1995; accepted 10 February 1997.

1. Bagnold, R. A. *The Physics of Blown Sand and Desert Dunes* (Chapman & Hall, London, 1941).
2. Jaeger, H. M. & Nagel, S. R. Physics of the granular state. *Science* **255**, 1523–1531 (1992).
3. Herrmann, H. J. in *Disorder and Granular Media* (eds Bideaux, D. & Hansen, A.) 305–320 (North-Holland, Amsterdam, 1993).
4. Edwards, S. F. in *Granular Matter: An Interdisciplinary Approach* (ed. Mehta, A.) 121–140 (Springer, New York, 1994).
5. Wolf, D. E. in *Computational Physics: Selected Methods, Simple Exercises, Serious Applications* (eds Hoffman, K. H. & Schreiber, M.) 64–95 (Springer, Berlin, 1996).

6. Williams, J. C. The segregation of particulates materials. A review. *Powder Technol.* **15,** 245–251 (1976).
7. Rosato, A., Strandburg, K. J., Prinz, F. & Swendsen, R. H. Why the Brazil nuts are on top: size segregation of particulate matter by shaking. *Phys. Rev. Lett.* **58,** 1038–1040 (1987).
8. Gallas, J. A. C., Herrmann, H. J. & Sokolowski, S. Convection cells in vibrating granular media. *Phys. Rev. Lett.* **69,** 1371–1374 (1992).
9. Knight, J. B., Jaeger, H. M. & Nagel, S. R. Vibration-induced size separation in granular media: the convection connection. *Phys. Rev. Lett.* **70,** 3728–3731 (1993).
10. Zik, O., Levine, D., Lipson, S. G., Shtrikman, S. & Stavans, J. Rotationally induced segregation of granular materials. *Phys. Rev. Lett.* **73,** 644–647 (1994).
11. Clément, E., Rajchenbach, J. & Duran, J. Mixing of a granular material in a bi-dimensional rotating drum. *Europhys. Lett.* **30,** 7–12 (1995).
12. Cooke, W., Warr, S., Huntley, J. M. & Ball, R. C. Particle size segregation in a two-dimensional bed undergoing vertical vibration. *Phys. Rev. E* **53,** 2812–2822 (1996).
13. Brown, R. L. The fundamental principles of segregation. *J. Inst. Fuel* **13,** 15–19 (1939).
14. Bagnold, R. A. Experiments on a gravity-free dispersion of large solid spheres in a Newtonian fluid under shear. *Proc. R. Soc. Lond. A* **225,** 49–63 (1954).
15. Drahun, J. A. & Bridgwater, J. The mechanisms of free surface segregation. *Powder Technol.* **36,** 39–53 (1983).
16. Fayed, M. E. & Otten, L. (eds) *Handbook of Powder Science and Technology* 428–433 (Van Nostrand Reinhold, New York, 1984).
17. Savage, S. B. in *Developments in Engineering Mechanics* (ed. Selvadurai, A. P. S.) 347–363 (Elsevier, Amsterdam, 1987).
18. Savage, S. B. & Lun, C. K. K. Particle size segregation in inclined chute flow of dry cohesionless granular solids. *J. Fluid Mech.* **189,** 311–335 (1988).
19. Savage, S. B. in *Theoretical and Applied Mechanics* (eds Germain, P., Piau, M. & Caillerie, D.) 241–266 (Elsevier, Amsterdam, 1989).
20. Meakin, P. A simple two-dimensional model for particle segregation. *Physica A* **163,** 733–746 (1990).
21. Bagnold, R. A. The shearing and dilation of dry sand and the 'singing' mechanism. *Proc. R. Soc. Lond. A* **295,** 219–232 (1966).
22. Jaeger, H. M., Liu, C.-H. & Nagel, S. R. Relaxation at the angle of repose. *Phys. Rev. Lett.* **62,** 40–43 (1989).
23. Makse, H. A., Cizeau, P. & Stanley, H. E. Possible stratification mechanism in granular mixtures. *Phys. Rev. Lett.* (submitted).
24. Williams, J. C. The segregation of powders and granular materials. *Univ. Sheffield Fuel Soc. J.* **14,** 29–34 (1963).
25. Williams, J. C. The mixing of dry powders. *Powder Technol.* **2,** 13–20 (1968).
26. Allen, J. R. L. *Sedimentary Structures: their Character and Physical Basis* (Elsevier, Amsterdam, 1982).
27. Boutreux, T. & de Gennes, P.-G. Surface flows of granular mixtures: I. General principles and minimal model. *J. Phys. I France* **6,** 1295–1304 (1996).
28. Bouchaud, J.-P., Cates, M. E., Prakash, J. R. & Edwards, S. F. Hysteresis and metastability in a continuum sandpile model. *Phys. Rev. Lett.* **74,** 1982–1985 (1995).
29. de Gennes, P.-G. Dynamique superficielle d'un matériau granulaire. *C. R. Acad. Sci.* **321** [**IIb**], 501–506 (1995).

Acknowledgements. We thank T. Boutreux, G. Davies, P.-G. de Gennes, H. J. Herrmann and S. Tomassone for valuable discussions, P. Cizeau for collaboration in stages of this work, K, Papworth for technical assistance with the photographs, and BP for financial support.

Correspondence should be addressed to H.A.M. (hmakse@miranda.bu.edu).

Closure of the Central American Isthmus and its effect on deep-water formation in the North Atlantic

Kevin W. Burton*†, Hong-Fei Ling*‡ & R. Keith O'Nions*

* *Department of Earth Sciences, University of Oxford, Parks Road, Oxford OX1 3PR, UK*
‡ *Department of Earth Sciences, University of Nanjing, Nanjing 210008, China*

Modern ocean thermohaline-driven circulation influences global climate by transporting heat to high latitudes[1,2] and by affecting the exchange of CO_2 between ocean and atmosphere[3]. North Atlantic Deep Water (NADW) plays a key role in this circulation, and Quaternary climate cycles have been linked to changes in NADW flow[4]. General circulation model simulations indicate that before closure, some 3–4 million years ago, of the Central American Isthmus—the narrow strip of land linking North and South America—the direct flow of low-salinity water from the Pacific to the Atlantic Ocean would have led to a smaller NADW flow[5,6]. Sedimentation patterns[7] and nutrient proxies[8–11] support these model results by indicating an increase in NADW flow around the time of isthmus closure, but these records do not allow changes in different NADW sources to be distinguished, and the overall effect of closure on global ocean circulation is poorly known. Here we present Nd, Pb and Sr isotope records preserved by a hydrogenous ferromanganese crust from the NADW flow-path in the western North Atlantic Ocean. These records indicate that the isotopic signal associated with NADW strengthened around 3–4 million years ago showing that deep water that formed in the Labrador Sea made a gradually increasing contribution to NADW flow. These data, taken together with those from the central Pacific Ocean[12], indicate an increased NADW flow since isthmus closure, and suggest that the closure established today's general pattern of ocean circulation.

North Atlantic Deep Water possesses a distinct physical, chemical and isotopic signature (see, for example, refs 4, 13–15). In particular, the sources of NADW impart an extremely unradiogenic Nd isotope composition ($\epsilon_{Nd} = -13.5 \pm 0.5$ (ref. 15), where ϵ_{Nd} is the measured $^{143}Nd/^{144}Nd$ ratio relative to the chondrite uniform reservoir[16]; see Fig. 2a legend) which reflects local input through erosion of old continental material, consistent with the age of the surrounding land masses. By comparison, Antarctic Bottom Water (AABW), the only other major source of deep water in the present-day Atlantic, has a much more radiogenic Nd isotope composition ($\epsilon_{Nd} = -8.6 \pm 0.5$)[17]. These differences in isotopic composition ($\Delta\epsilon_{Nd} = 4.9 \pm 1.0$) are much larger than the present-day measurement precision for the $^{143}Nd/^{144}Nd$ ratio (± 20 p.p.m. (2σ) $\approx 0.20\,\epsilon_{Nd}$). Therefore, in principle, if an appropriate record can be found, it should be possible to detect the variations in seawater chemistry that would occur as a consequence of changes in deep-water circulation.

Hydrogenous ferromanganese crusts grow by direct accumulation of metal oxides from sea water, and thus potentially preserve a record of the chemistry of the sea water from which they grow. Here we present Nd, Pb and Sr isotope data for an Fe–Mn crust (BM1969.05) from the San Pablo seamount in the western North Atlantic (Table 1) which lies close to the path of the Deep Western Boundary Current (the southern extension of NADW) and, hence, should sample 'well mixed' NADW on its passage south. The crust is up to 120 mm thick, shows no phosphatization ($P \leq 0.4\%$; compare refs 12, 18) and little elemental variation, except for Al which shows a distinct break 58 mm from the outer surface (Fig. 1a). Crust sampling and isotopic analysis follows procedures reported elsewhere[12], and isotopic data are given in Table 1. $\Delta^{87}Sr$ ages (Fig. 1b), calculated using Sr isotope stratigraphy[19–22], indicate that the crust started to grow some 18 Myr ago, and preserves two distinct growth intervals. The first, from 18.2 ± 0.6 to 16.2 ± 0.6 Myr ago and the second, from around 10.2 ± 1.2 Myr ago to the present day. The marked break at 58 mm corresponds to a hiatus of some 6.0 Myr, and correlates with the shift in Al, relating either to cessation of growth or an interval of crust erosion. Crust precipitation is considered to occur when oxygen-rich deep water is brought into contact with Mn^{2+}-rich water from the oxygen minimum zone. It is interesting to note that the two phases of crust growth correspond to periods when oxygen-rich NADW[14] is considered to have been actively formed[8]. The outer surface does not yield any useful age information, giving an $^{87}Sr/^{86}Sr$ ratio much more radiogenic than the present-day value for sea water, possibly due to the incorporation of detrital phases, or surface contamination during sampling. However, a $^{234}U/^{238}U$ age of 8 ± 0.3 kyr for the same sample[23] indicates that there was no significant break in growth, or loss of material. The sample contains no detectable secondary phases, or evidence for diagenesis, although it is not possible to rule out the possibility of isotopic homogenization after growth. However, the preservation of a major growth hiatus that correlates with the break in Al concentration, taken with the systematic nature of the $\Delta^{87}Sr$ ages, suggests that there has been no significant perturbation of the elemental record. Thus, the ages can be

† Present address: Laboratoire de Géochimie et Cosmochimie, CNRS URA 1758, IPG-Paris, 4 Place Jussieu, 75252 Paris Cedex 05, France.